Experimental studies of circular attractors in the first rf-based electron cooler

S. Seletskiy,* A. Fedotov, and D. Kayran
Brookhaven National Laboratory, Upton, New York 11973, USA

(Received 11 October 2022; accepted 26 January 2023; published 8 February 2023)

In electron coolers, under certain conditions, a circular attractor (CA) can appear in either a longitudinal or a transverse phase space of cooled ion bunches. In the presence of an attractor, ions with small amplitudes of synchrotron or betatron oscillations are getting excited rather than being damped. This effect was observed at several nonrelativistic electron coolers with a direct current electron beam. Experimental studies of circular attractors at electron coolers utilizing rf-accelerated electron bunches, where this effect becomes particularly important, are lacking. We report CA studies at the low energy RHIC electron cooler (LEReC)—the first rf-based relativistic electron cooler. We derive formulas defining conditions for a CA appearance, perform dedicated experiments, and compare the measurements' results to the theoretical predictions.

DOI: 10.1103/PhysRevAccelBeams.26.024401

I. INTRODUCTION

Electron cooling [1,2] is a method of increasing a phase space density of hadron bunches in storage rings.

In electron cooling, ions co-propagate with an electron beam with the same average velocity in the straight section of a storage ring called the cooling section (CS). The electron beam is either discarded or decelerated and recuperated after each passage through the CS. Hence, the ions interact with fresh electrons on each turn. Cold electron "gas" interacts with the ions via Coulomb force. This results in a dynamical friction [3] reducing the ions' momentum spread in the comoving beam frame. In a laboratory frame, this cooling process is observed as a reduction in both transverse and longitudinal emittances of the ion bunch over many revolutions in the ring.

If the relative offset in average velocities of an electron beam and ion bunches in the CS exceeds some critical value, then the resulting friction force creates a circular attractor in the phase space of the ion bunch. The attractor excites oscillations of ions with small synchrotron or betatron amplitudes, thus, turning cooling into "anticooling."

This effect was predicted [4] and observed at several nonrelativistic (with a relativistic factor $\gamma \approx 1$) coolers [5,6]. It was recently discovered that a similar effect is expected in coherent electron coolers, as well [7].

All nonrelativistic electron coolers utilize a dc electron beam and use beam "magnetization," i.e., both the electron gun's cathode and the cooling section in such a cooler are immersed into a solenoidal magnetic field. The first relativistic electron cooler [8] was also using a magnetized dc electron beam.

The low energy RHIC electron cooler [9–14] is the first cooler that uses rf-accelerated electron bunches; it is also the first cooler with no beam magnetization. LEReC successfully provided cooling of colliding ions at $\gamma = 4.1$ and $\gamma = 4.9$ in RHIC.

The LEReC approach significantly simplifies the engineering design of relativistic coolers and allows the scaling of electron cooling to high energies. For example, the Electron Ion Collider (EIC) [15] precooler, which will be operated at $\gamma = 25.4$, is based on the LEReC design principles [16]. One of the two options considered for cooling the EIC protons at $\gamma = 293$ is also based on bunched, nonmagnetized electron cooling [17].

A critical average velocity offset, which results in an appearance of a circular attractor, is comparable to a root mean square (rms) velocity spread of an electron beam in a cooling section. Since the velocity distribution of a magnetized dc electron beam is substantially different from distribution in nonmagnetized electron bunches, the resulting implications of the circular attractor (CA) driven dynamics for performances of traditional and rf-based coolers are drastically different.

The relative energy spread of a dc electron beam is much smaller than the spread of ions, and effective angles of magnetized electrons are defined by a uniformity and an alignment of the CS magnetic field (both well-controlled parameters). Hence, the critical velocity offset (v_c) in

*seletskiy@bnl.gov

respective coolers is much smaller than the velocity spread of an ion bunch, and if an average velocity mismatch of the two beams exceeds v_c, the resulting attractor is much smaller than the ion bunch's velocity spread. Such an attractor is not damaging to cooling and can be even used beneficially, for example, to make cooling more uniform in a wider range of synchrotron amplitudes [18].

On the other hand, in rf-based nonmagnetized electron coolers, velocity spreads of electron bunches are comparable to the respective ion bunches' spreads. Therefore, mismatches in the average velocities of the beams exceeding the critical value create an attractor, which completely destroys cooling. Just as important, CA-driven requirements to the coolers' design become tighter, the higher the electron beam energy is.

These considerations make experimental characterization of circular attractors in relativistic, rf-based coolers particularly consequential. Such studies were recently performed at LEReC and are reported in this manuscript.

In the next section, we revisit the theory behind the formation of circular attractors and derive useful formulas for simulations and numerical estimates of the respective effects.

In Sec. III, we describe the first experimental studies of circular attractors in the bunched nonmagnetized electron cooler and compare CA studies to the theory derived in Sec. II.

In Sec. IV, implications of the circular attractor theory for design parameters of the EIC coolers are discussed.

II. THEORETICAL CONSIDERATIONS

In nonmagnetized coolers, the friction force acting on an ion in a beam frame is given by [19,20]:

$$\vec{F}(\vec{v}_i) = C_0 \int L_C \frac{\vec{v}_i - \vec{v}_e}{|\vec{v}_i - \vec{v}_e|^3} f(\vec{v}_e, \vec{\mu}) d^3 v_e \qquad (1)$$

Here, $C_0 = -\frac{4\pi n_e e^4 Z^2}{m_e}$, n_e is the electron bunch density in the beam frame, e is the electron charge, Ze is the ion charge, m_e is the mass of the electron, $\vec{v}_i$ and $\vec{v}_e$ are ion and electron velocities in the beam frame. The Coulomb logarithm is $L_C = \ln(\rho_{\max}/\rho_{\min})$ with a minimal impact parameter $\rho_{\min} = (Ze^2)/(m_e|\vec{v}_i - \vec{v}_e|^2)$. A maximum impact parameter $\rho_{\max}$ is determined by the time of flight of the ions through the CS. The Coulomb logarithm can be assumed to be constant. It is assumed that the velocity distribution of the electron bunch $f(\vec{v}_e, \vec{\mu})$ has an offset $\vec{\mu}$ with respect to the zero velocity in the ion beam frame. In the laboratory frame, the longitudinal velocity offset (μ_z) corresponds to an offset in the relative momentum of the electron beam: $\Delta\delta = \frac{\mu_z}{\beta c}$, where c is the speed of light and β is a relativistic factor. For a transverse direction, horizontal and vertical velocity offsets (μ_x and μ_y) correspond to a respective angular misalignment between the electron and ion beam trajectories: $\theta_{x,y} = \frac{\mu_{x,y}}{\gamma\beta c}$.

Each component (F_x, F_y, F_z) of the friction force (1) can be represented by a 1D integral, which substantially simplifies numerical studies of the dynamics of the ion-electron interactions. Such expressions (known as Binney's formulas [21]) can be obtained under the assumption of Maxwell-Boltzmann distribution $f(\vec{v}_e, \vec{\mu})$:

$$f(\vec{v}_e, \vec{\mu}) = \frac{e^{-\frac{(v_{ex}-\mu_x)^2}{2\sigma_{v_{ex}}^2}} e^{-\frac{(v_{ey}-\mu_y)^2}{2\sigma_{v_{ey}}^2}} e^{-\frac{(v_{ez}-\mu_z)^2}{2\sigma_{v_{ez}}^2}}}{(2\pi)^{3/2}\sigma_{v_{ex}}\sigma_{v_{ey}}\sigma_{v_{ez}}} \qquad (2)$$

Here $\sigma_{v_{ex}}$, $\sigma_{v_{ey}}$, and $\sigma_{v_{ez}}$ are, respectively, the horizontal, the vertical, and the longitudinal rms velocity spreads of the electron bunch in the beam frame.

We introduce an effective potential in a velocity space:

$$U = C_0 \int \frac{f(\vec{v}_e, \vec{\mu})}{|\vec{v}_i - \vec{v}_e|} d^3 v_e \qquad (3)$$

such that $F_{x,y,z} = \partial U/\partial v_{x,y,z}$. Then, substituting Eq. (2) into Eq. (3), after some algebraic manipulations [22], we obtain

$$\begin{cases} F_{x,y} = -C(v_{ix,y} - \mu_{x,y}) \int_0^\infty \frac{E}{\sigma_{v_{et}}^2 (1+q)^2 \sqrt{\sigma_{v_{et}}^2 q + \sigma_{v_{ez}}^2}} dq \\ F_z = -C(v_{iz} - \mu_z) \int_0^\infty \frac{E}{(1+q)(\sigma_{v_{et}}^2 q + \sigma_{v_{ez}}^2)^{3/2}} dq \end{cases} \qquad (4)$$

where $E = \exp\left[-\frac{(v_{ix}-\mu_x)^2 + (v_{iy}-\mu_y)^2}{2\sigma_{v_{et}}^2(1+q)} - \frac{(v_{iz}-\mu_z)^2}{2(\sigma_{v_{et}}^2 q + \sigma_{v_{ez}}^2)}\right]$, $C = 2\sqrt{2\pi} n_e r_e^2 m_e c^4 Z^2 L_C$, r_e is the classical electron radius, and $\sigma_{v_{ex}} = \sigma_{v_{ey}} \equiv \sigma_{v_{et}}$.

In the following considerations, we assume that the velocity offset has only a longitudinal nonzero component. This corresponds to the experimental setup described in the next section. Nonetheless, all the conclusions derived for $\mu_z \neq 0$ are equally applicable to the nonzero transverse velocity offsets as well [23].

Figure 1 shows a longitudinal component of the friction force for $\mu_z \neq 0$. Below, we study the effect that the shifted force has on the longitudinal dynamics of the ion bunch.

The longitudinal motion of an individual ion in the linear part of the rf bucket is given by

$$\begin{cases} \tau' = \delta \\ \delta' = -\tau + K(\tau, \delta). \end{cases} \qquad (5)$$

Here $\delta = \frac{v_{iz}}{\beta c}$ is the ion's relative momentum, $\tau = z/\beta_z$, z is the ion's longitudinal position with respect to the center of the rf bucket, $\beta_z = \eta\beta c/\omega_s$ is a longitudinal β function, ω_s is a synchrotron frequency, η is a slip factor of the ion storage ring, $\tau' \equiv d\tau/d\phi$, $\delta' \equiv d\delta/d\phi$, and ϕ is the synchrotron phase.

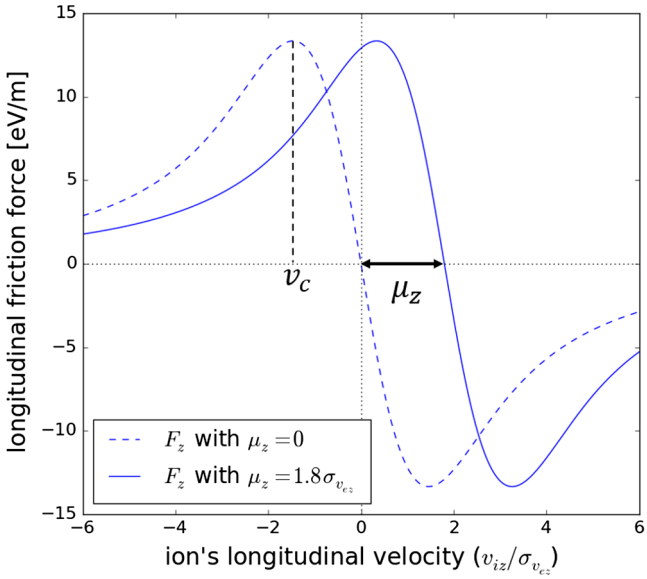

FIG. 1. Dependence of the longitudinal friction force on an ion's longitudinal velocity (relative to the electron bunch's rms velocity spread) in the case of the nonzero longitudinal velocity offset (the blue solid line) and in the case of $\mu_z = 0$ (the blue dashed line). It is assumed that the ion's transverse velocity is equal to the rms transverse velocity spread of the ion bunch. The force is calculated for the LEReC and RHIC parameters used in the experiment listed in Table I.

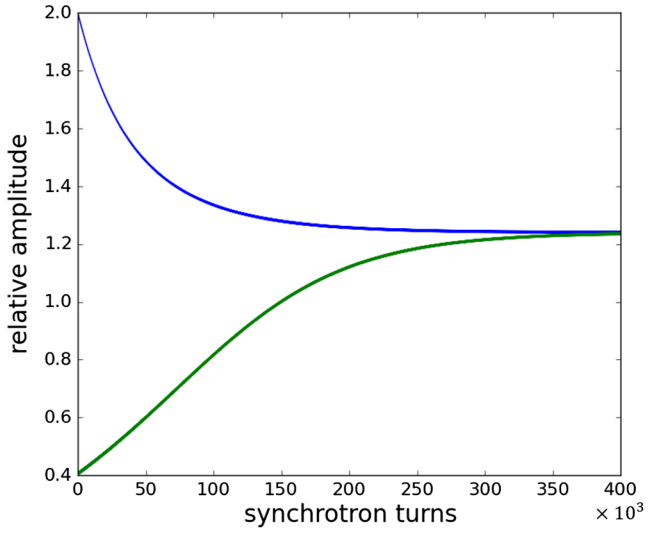

FIG. 2. Evolution of the relative amplitude of synchrotron oscillations under the influence of the friction force shown in Fig. 1. The oscillations of the ion with initial amplitude $j_0 = 0.4$ are getting excited (the green line), and the oscillations of the ion with $j_0 = 2$ are getting damped (the blue line). Both ions reach a nonzero equilibrium oscillations amplitude in approximately 4×10^5 synchrotron turns.

We are considering electron cooling using a bunched electron beam. For such a cooler, it is typical for an ion bunch to be overlapped with N electron bunches with a length that is much shorter than the ion bunch length. Therefore, a relative momentum "kick" due to the ion's interaction with the electron bunch is

$$K(\tau,\delta) = \alpha \mathbb{C}(\tau) \frac{F_z(\delta\beta c) L_{cs}}{\beta^2 \gamma m_i c^2}, \tag{6}$$

where L_{cs} is the length of the cooling section, m_i is the ion's mass, the coefficient $\alpha = \frac{l_e}{2\pi Q_s \beta_z |\delta|}$ is the number of times an ion with a given $|\delta|$ lands on the e-bunch, l_e is the electron bunch full width at half maximum, Q_s is the synchrotron tune, and a comb function $\mathbb{C}$ is given by

$$\mathbb{C}(\tau) = \sum_n^N \delta_D\left(\tau - \frac{z_{en}}{\beta_z}\right). \tag{7}$$

Here δ_D is a Dirac delta function and z_{en} is the longitudinal position of the nth electron bunch with respect to the center of the ion bunch.

Equation (5) with the friction force in the form (4) can be integrated numerically with a third order method [24].

Figure 2 shows an evolution of a relative oscillation amplitude $j = \sqrt{\tau^2 + \delta^2}/\sigma_{\delta i0}$ of the two ions under the influence of the friction force shown in Fig. 1 (here $\sigma_{\delta i0}$ is the initial rms momentum spread of the ion bunch). While the oscillations of the ion with the initial relative amplitude $j_0 = 2$ are getting damped, the ion with $j_0 = 0.4$ is getting excited, until both ions start oscillating with the same amplitude.

This behavior is caused by the presence of a circular attractor in the ions' phase space. The necessary and sufficient conditions for the formation of an attractor is that an oscillator experiences a force, which is a non-monotonic function of velocity, and which is offset with respect to $v = 0$ by a value larger than the critical velocity (v_c) defined by

$$\left.\frac{dF_z}{dv}\right|_{v_c} = 0. \tag{8}$$

As an example, Eq. (8) applied to the friction force from Fig. 1 gives $v_c = 1.46\sigma_{ez}$, and since we chose $\mu_z = 1.8\sigma_{ez}$ (i.e., $\mu_z > v_c$), F_z creates the circular attractor in the longitudinal phase space.

The mechanism of an attractor formation is easy to understand if we remember that during the synchrotron oscillations, each ion "meets" the electron bunches both when the ion's relative momentum is positive and when $\delta < 0$. Then the average friction force experienced by the ion is $\langle F_z \rangle = [(F_z(v_z) - F_z(-v_z)]/2$. Figure 3 shows the effective average friction force acting on the ions for the case of Fig. 1.

As one can see, the average force in the range of $[-v_a, v_a]$ is codirected with the ion velocity. Hence, it is

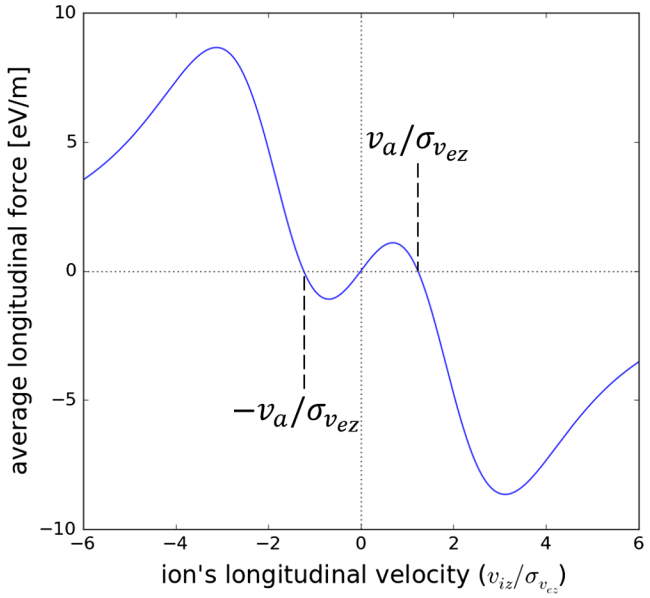

FIG. 3. Effective average friction force acting on the ions.

exciting oscillations for the ions with $j < v_a/(\beta c\sigma_{\delta i0})$. For the amplitudes outside of this range, the friction force is damping the oscillations. The equilibrium oscillation amplitude $j_a = v_a/(\beta c\sigma_{\delta i0})$ gives the radius of the attractor and is defined by

$$F_z(v_a) = F_z(-v_a). \tag{9}$$

The CA effect on the dynamics of the ion bunch is demonstrated in Fig. 4, which shows the resulting ions' distribution in the longitudinal phase space developed under the influence of the offset friction force. All the ions gravitate to the same synchrotron amplitude (j_a), thus forming a doughnut-shaped distribution in the phase space. This produces a two-hump longitudinal density distribution of the ion bunch. Notice, that in the presented simulations we introduced a noise emulating the diffusion caused by the intrabeam scattering (IBS). Without such a noise, the ions eventually form an ideal circle of radius j_a in the (τ, δ)-plot.

In the conclusion of this section, let us reiterate that formulas (8) and (9) are applicable to transverse directions as well as to longitudinal ones. To obtain a critical velocity or an attractor radius in either a horizontal or a vertical plane, one simply must substitute F_z in Eqs. (8) and (9) with a respective (F_x or F_y) component of the friction force. Such formulas will be used in Sec. IV to find requirements for the relative angular alignment of electron and ion beams in the EIC coolers.

In the next section, we will describe the experimental studies of the CA formation in the first rf-based non-magnetized cooler and compare our measurements to the analytic formulas derived above.

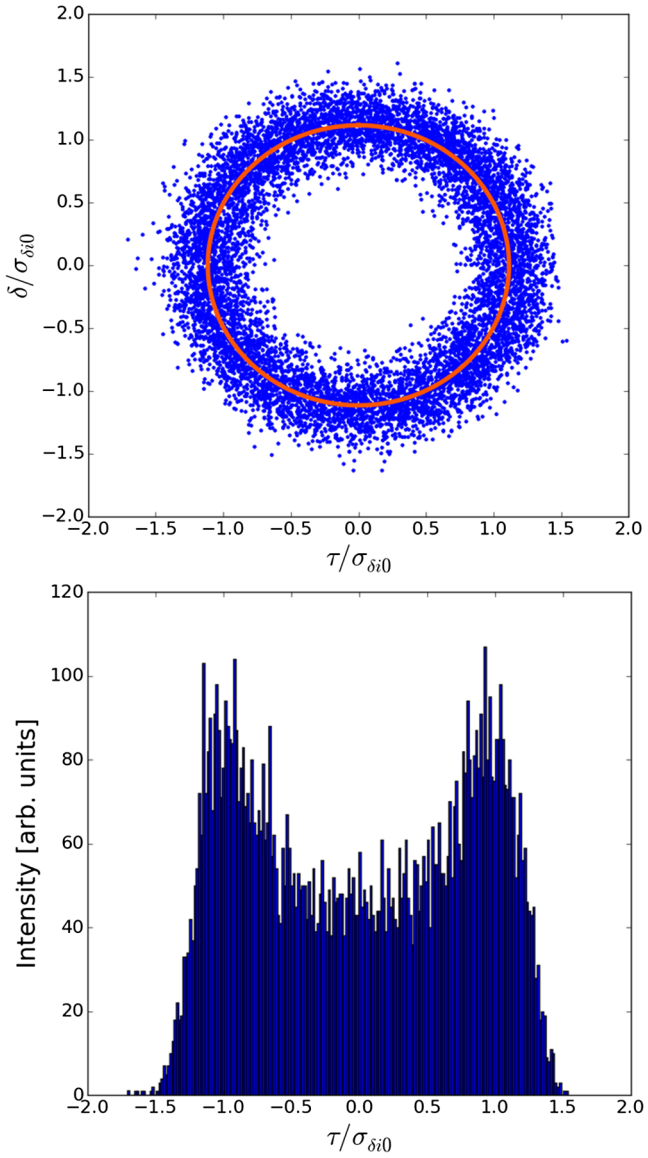

FIG. 4. The ions' distribution in the presence of the circular attractor. In the simulations, the ion bunch has a Gaussian initial distribution with the rms energy spread $\sigma_{\delta i0}$. The ions are tracked for 4×10^5 synchrotron turns under the influence of the offset friction force shown in Fig. 1. The solid red line shows the location of the attractor of radius $j_a = v_a/(\beta c\sigma_{\delta i0})$ with v_a found from Eq. (9).

III. EXPERIMENTAL STUDIES OF CIRCULAR ATTRACTORS IN LEREC

The LEReC layout is shown in Fig. 5.

The LEReC photocathode is illuminated by a green 704-MHz laser modulated with a 9-MHz frequency to match the frequency of RHIC ions. The resulting 9-MHz "macro-bunches" of the electrons consist of thirty 704 MHz bunches each. When overlapped with the ion bunch in the cooling section, the electron macrobunch covers $\pm 2\sigma_{zi0}$ of the longitudinal span of the ion bunch (see Fig. 6).

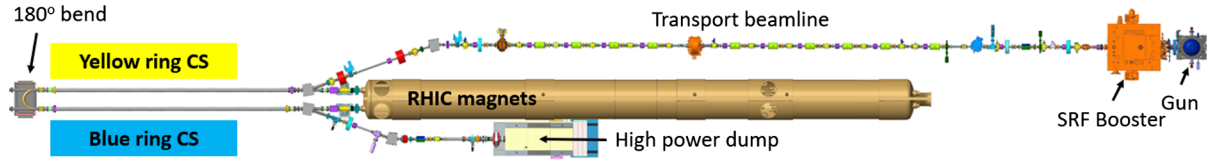

FIG. 5. Schematics of LEReC layout (not to scale).

The electrons are accelerated to 375 keV in the dc gun [12] followed by a 704-MHz superconducting rf accelerating cavity (SRF Booster) [25] bringing the beam energy to 1.6–2. MeV. The electron beam is transported in a 40-m long transport beamline and merged to the cooling section in the "Yellow" RHIC ring via the merger dogleg. After passing the Yellow CS, the beam is sent to the cooling section in the "Blue" RHIC ring by a 180° bend. Finally, the electron beam is extracted at the exit of the blue CS through the extraction dogleg and sent to the beam dump.

For the operational RHIC conditions, the IBS-driven diffusion rate in the ion bunches is comparable to the cooling rate provided by LEReC. Therefore, in operations, the presence of the CA effect on the ion bunches is observed only as a growth of the effective rms length (or of the transverse emittance, if the attractor is formed in the transverse phase space) of the ion bunch and is indistinguishable from extra heating.

Another important factor complicating CA observations is that the cooling time in LEReC is several minutes rather than seconds (or subseconds) typical for nonrelativistic coolers.

All of that makes observing a clear two-hump density distribution caused by a CA particularly challenging at LEReC and requires a special experimental setup.

In the dedicated CA measurements, we utilized the low intensity ion bunches (with about 2×10^8 ions per bunch) in the Yellow RHIC ring. For such ion bunches, the longitudinal IBS diffusion rate is $\approx 10^{-3}$ 1/s. On the other hand, the longitudinal cooling rate in the experiment was $\approx 3.5 \times 10^{-3}$ 1/s.

During the experiment, we ran LEReC in a special 76-kHz mode. In that mode, several consecutive 9-MHz macrobunches of electrons are generated with the 76-kHz frequency, which corresponds to the RHIC revolution frequency. The macrobunches generated in the 76 kHz mode have different average energies, which is caused by the rf beam loading. Therefore, such a configuration provides simultaneous interaction of ion bunches with electron bunches of varying energy offset.

The described setup allowed us to observe the formation of a two-hump distribution indicative of the presence of the circular attractor.

Table I lists the parameters used in the experiment.

Figure 7 shows the CA measurements for the relative energy offset of 10.1×10^{-4}. The three profiles in Fig. 7 show the 20-min worth of the evolution of the longitudinal distribution of the ion bunch. Due to a poor lifetime of the ions in RHIC at this energy, the ion bunch intensity dropped by about a factor of 2 during the measurement.

Figure 8 compares the final distribution obtained in Fig. 7 to the distribution obtained in simulations run with the parameters of the experiment. Comparison of distributions obtained in other measurements to respective simulations provides the same level of agreement.

The relative radius of the attractor $(v_a/\sigma_{v_{ez}})$ can be calculated from a measured distance (Δt_a) between peaks of the two-hump distribution

$$\frac{v_a}{\sigma_{v_{ez}}} = \frac{\omega_s \Delta t_a}{\eta \sigma_{v_{ez}}}. \tag{10}$$

Figure 9 shows a comparison of the circular attractor's radius calculated from the measurements to the results of the theoretical formula (9) with the longitudinal friction

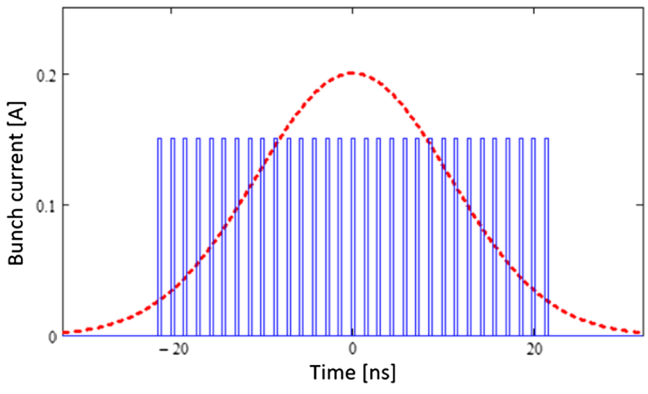

FIG. 6. Longitudinal distribution of the ion bunch (dashed red line) overlapped with the electron macrobunch (solid blue line) containing 30 bunches.

TABLE I. Beam parameters in CA experiment.

Relativistic γ	4.1
Number of ions per bunch	2×10^8
Initial rms length of i-bunch (ns)	18
Number of e-bunches per macrobunch	36
e-bunch's charge (pC)	36.1
Electrons' rms relative momentum spread	5×10^{-4}
Electron's rms angular spread (μrad)	150
e-bunch's FWHM length (ps)	300

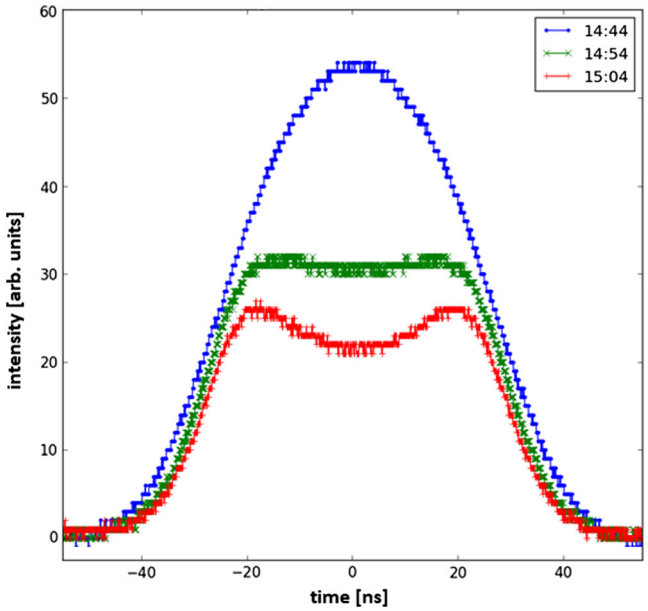

FIG. 7. Evolution of the longitudinal distribution of the ion bunch in the presence of the circular attractor.

force calculated according to Eq. (4). The error bars in Fig. 9 are defined by the accuracy of the measurements of both the average energy of the electron bunch and the e-bunch energy spread, as well as the resolution of the measurement of the i-bunch's longitudinal profile.

Figure 9 demonstrates that the formulas derived in the previous section are in good agreement with the experimental data. In the next section, we will apply this theory to the EIC coolers.

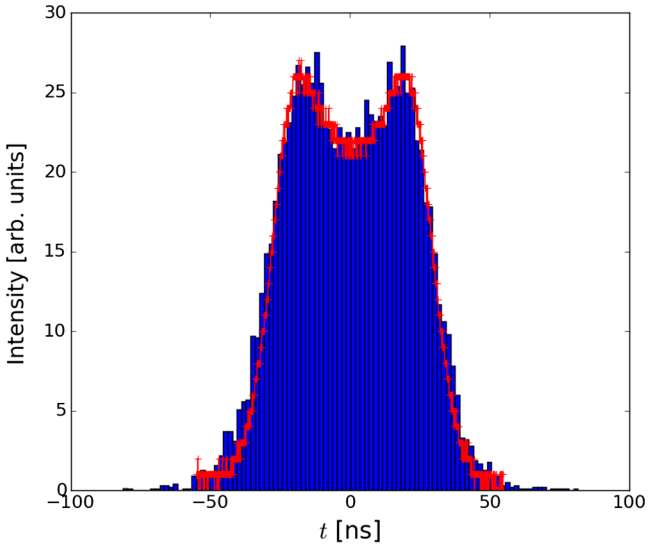

FIG. 8. Comparison of the experimentally measured final distribution of Fig. 7 (red trace) to the simulations (blue histogram) performed with the parameters used in the experiment. The intensity of the simulated distribution is an adjustable parameter.

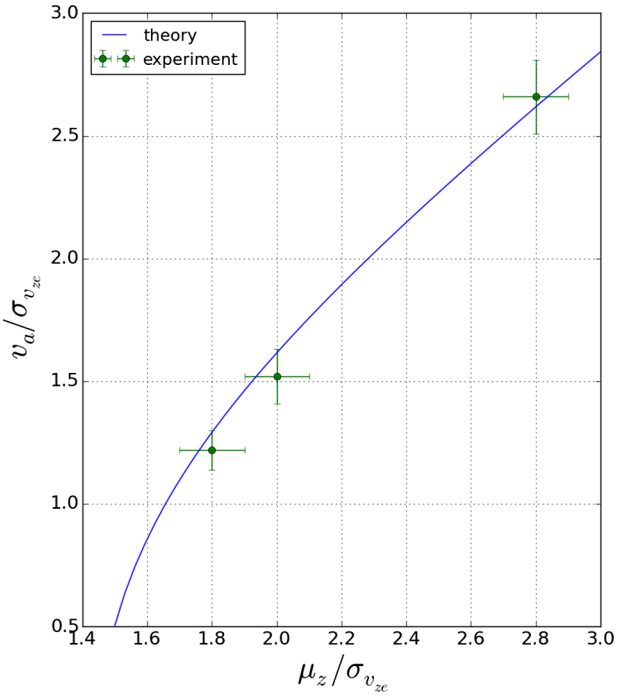

FIG. 9. Theoretical and experimentally measured radius of a circular attractor in the ions' longitudinal phase space created by a constant offset of the electron beam energy.

IV. REQUIREMENTS FOR EIC COOLERS

The Electron Ion Collider requires a precooling of protons at an injection energy ($\gamma = 25.4$) prior to bringing them up to a collision energy. The precooler [16] is designed to cool vertical normalized emittance of proton bunches from 2 to 0.45 mm mrad on a time scale of 30–50 min.

The precooler is based on LEReC technology, it utilizes rf-accelerated nonmagnetized electron bunches. The most recent precooler parameters relevant to our considerations are listed in Table II.

Substituting parameters listed in Table II into Eq. (4), we obtain the friction force shown in Fig. 10.

Applying Eq. (8) to the respective components of the calculated friction force, we find that for the horizontal and vertical directions, the critical velocity offsets are equal to $1.4\sigma_{v_{e(x,y)}}$. Converting velocity offset to an angle, we find that the requirement to a relative angular alignment

TABLE II. Parameters of the EIC cooler operating at $\gamma = 25.4$.

Cooling section length (m)	120
Initial protons normalized emittance (x,y) (μm)	2, 2
Protons β function (x,y) in CS (m)	200, 200
Protons relative momentum spread	6×10^{-4}
Number of e-bunches per proton bunch	2
e-bunch's charge (nC)	2
Electron's rms angular spread (μrad)	20
Electrons' rms relative momentum spread	5×10^{-4}

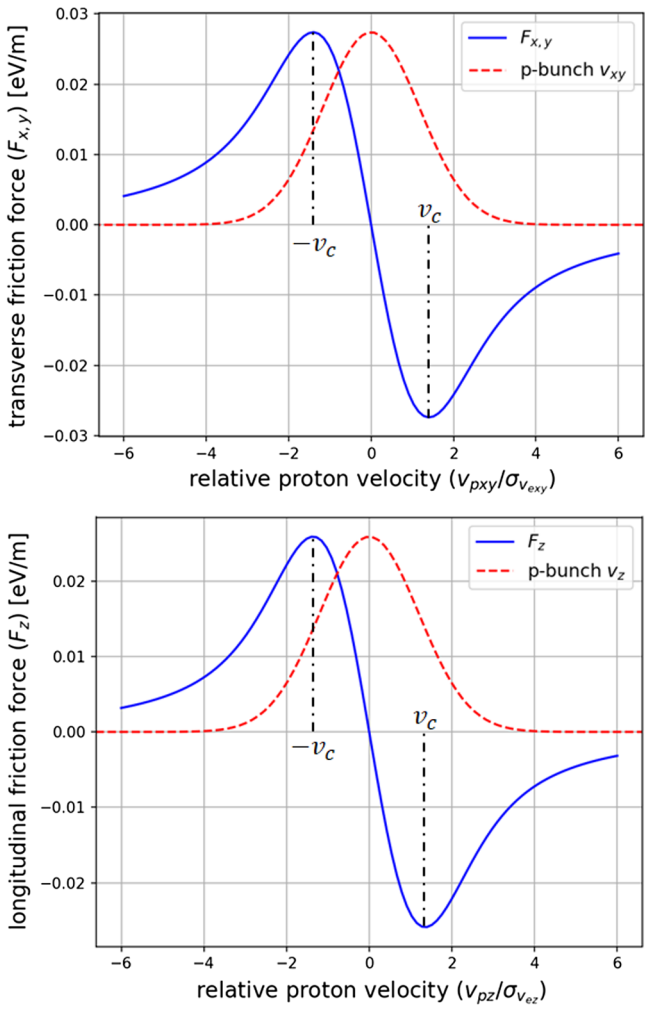

FIG. 10. Transverse and longitudinal components of the friction force in the EIC precooler (solid blue line). Respective velocity distributions of protons are shown for comparison (red dashed line). The values of critical velocity mismatches are marked by v_c.

of the electron and proton beam trajectories is $\theta_{x,y} < \frac{1.4\sigma_{v_{e(x,y)}}}{\gamma\beta c} \approx 28$ μrad.

Similarly, the critical velocity in the longitudinal direction is $1.3\sigma_{v_{ez}}$. Converting this value to a tolerable error in the setting of electron beam energy, we get $\Delta\delta < \frac{1.3\sigma_{v_{ez}}}{\beta c} \approx 6.5 \times 10^{-4}$.

One of the possibilities for compensating an IBS-driven emittance growth of proton bunches during an EIC operation, at $\gamma = 293$, is an Electron Ring Cooler [17]. The Ring Cooler is also based on cooling with nonmagnetized electron bunches. Its main difference from other coolers is that the electron bunches are stored for several seconds in an electron storage ring and reused for cooling on numerous turns. An emittance growth of the electron bunches both due to their interaction with the protons and due to the IBS is compensated by a radiation damping facilitated by damping wigglers.

TABLE III. Parameters of the EIC cooler operating at $\gamma = 293$.

Cooling section length (m)	170
Protons normalized emittance (x,y) (μm)	3.3, 0.3
Protons β function (x,y) in CS (m)	170, 1900
Protons relative momentum spread	6.8×10^{-4}
Number of e-bunches per proton bunch	1
e-bunch's charge [nC]	16
Electron's rms angular spread [μrad]	9
Electrons' rms relative momentum spread	9×10^{-4}

The most recent parameters of the Ring Cooler are listed in Table III.

A calculation of alignment tolerances for the Ring Cooler gives $\theta_{x,y} < 11$ μrad and $\Delta\delta < 1.46 \times 10^{-3}$.

The studies performed in this section provide alignment tolerances required to observe at least some cooling and are critically important for the commissioning of the coolers. Operation of the coolers might require even tighter alignment tolerances, which will be defined as a part of an overall "alignment budget" at later stages of the design.

Finally, let us repeat that the requirements for an angular alignment of the beams become tighter, the higher a cooler's energy is. For comparison, at LEReC with $v_c \approx 1.4\sigma_{v_{e(x,y)}}$, the requirement for the initial angular alignment of the beams was $\theta_{xy} < 200$ μrad.

V. CONCLUSION

In this paper, we present the first experimental studies of the formation of circular attractors in a relativistic rf-based electron cooler. The formulas for the evaluation of conditions resulting in the appearance of an attractor and for the calculation of the attractor's radius were derived. The experimental results were found to be in good agreement with the theory. The derived formulas were applied to define tolerances to the relative alignment of the electron and proton beams in the coolers currently designed for the Electron-Ion Collider.

ACKNOWLEDGMENTS

This work was supported by Brookhaven Science Associates, LLC under Contract No. DE-SC0012704 with the U.S. Department of Energy.

[1] G. I. Budker, An effective method of damping particle oscillations in proton and antiproton storage rings, At. Energy **22**, 346 (1967) [Sov. At. Energy **22**, 438 (1967)].
[2] G. I. Budker *et al.*, Experimental study of electron cooling, Part. Accel. **7**, 197 (1976).
[3] S. Chandrasekhar, Brownian motion, dynamical friction and stellar dynamics, Rev. Mod. Phys. **21**, 383 (1949).

[4] Ya. S. Derbenev and A. N. Skrinsky, The kinetics of electron cooling of beams in heavy particle storage rings, Part. Accel. **8**, 1 (1977).

[5] D. D. Caussyn *et al.*, Negative Resistance Instability due to Nonlinear Damping, Phys. Rev. Lett. **73**, 2696 (1994).

[6] K. Rathsman, Modelling of electron cooling: Theory, data and applications, Ph.D. thesis, Uppsala University, 2010.

[7] S. Seletskiy, A. Fedotov, and D. Kayran, Circular attractors as heating mechanism in coherent electron cooling, Phys. Rev. Accel. Beams **25**, 054403 (2022).

[8] S. Nagaitsev *et al.*, Experimental Demonstration of Relativistic Electron Cooling, Phys. Rev. Lett. **96**, 044801 (2006).

[9] A. Fedotov *et al.*, Experimental Demonstration of Hadron Beam Cooling Using Radio Frequency Accelerated Electron Bunches, Phys. Rev. Lett. **124**, 084801 (2020).

[10] D. Kayran *et al.*, High brightness electron beams for linac based bunched beam electron cooling, Phys. Rev. Accel. Beams **23**, 021003 (2020).

[11] S. Seletskiy *et al.*, Accurate setting of electron energy for demonstration of first hadron beam cooling with rf accelerated electron bunches, Phys. Rev. ST Accel. Beams **22**, 111004 (2019).

[12] X. Gu *et al.*, Stable operation of a high voltage high current dc photoemission gun for the bunched beam electron cooler in RHIC, Phys. Rev. Accel. Beams **23**, 013401 (2020).

[13] H. Zhao *et al.*, Cooling simulation and experimental benchmarking for an rf based electron cooler, Phys. Rev. Accel. Beams **23**, 074201 (2020).

[14] S. Seletskiy *et al.*, Obtaining transverse cooling with nonmagnetized electron beam, Phys. Rev. Accel. Beams **23**, 110101 (2020).

[15] Electron Ion Collider conceptual design report, edited by J. Beebe-Wang *et al.*, https://www.bnl.gov/ec/files/EIC_CDR_Final.pdf (2021).

[16] A. Fedotov, S. Benson *et al.*, Low-energy cooling for the Electron Ion Collider, Brookhaven National Laboratory (BNL), Upton, NY, Report No. BNL-220686-2020-TECH, 2020.

[17] H. Zhao, J. Kewisch, M. Blaskiewicz, and A. Fedotov, Ring-based electron cooler for high energy beam cooling, Phys. Rev. Accel. Beams **24**, 043501 (2021).

[18] Private conversations with Dr. A. Sidorin.

[19] S. Chandrasekhar, *Principles of Stellar Dynamics* (University of Chicago Press, Chicago, 1942).

[20] Ya. S. Derbenev and A. N. Skrinsky, The effect of an accompanying magnetic field on electron cooling, Part. Accel. **8**, 235 (1978).

[21] J. Binney, Dynamical friction in aspherical clusters, Mon. Not. R. Astron. Soc. **181**, 735 (1977).

[22] S. Seletskiy and A. Fedotov, Effects of coherent offset of velocity distribution in electron coolers on ion dynamics, Brookhaven National Laboratory (BNL), Upton, NY, Report No. BNL-220641-2020-TECH, 2020.

[23] S. Seletskiy, A. Fedotov, and D. Kayran, Coherent excitations and circular attractors in cooled ion bunches, in *Proceedings of the 12th International Particle Accelerator Conference, IPAC-2021, Campinas, SP, Brazil* (JACoW, Geneva, Switzerland, 2021), TUXA04.

[24] R. D. Ruth, IEEE Trans. Nucl. Sci. **NS-30**, 2669 (1983).

[25] B. Xiao *et al.*, Design and test of 704 MHz and 2.1 GHz normal conducting cavities for low energy RHIC electron cooler, Phys. Rev. Accel. Beams **22**, 030101 (2019).